



ELSEVIER

Available online at [www.sciencedirect.com](http://www.sciencedirect.com)

ScienceDirect

journal homepage: [www.elsevier.com/locate/he](http://www.elsevier.com/locate/he)

# Counter-intuitive reduction of thermal contact resistance with porosity: A case study of polymer electrolyte membrane fuel cells

Hamidreza Sadeghifar <sup>a,b,c,d,\*</sup>, Ned Djilali <sup>c</sup>, Majid Bahrami <sup>b</sup>

<sup>a</sup> Department of Chemical and Biological Engineering, University of British Columbia, 2360 East Mall, Vancouver, BC V6T 1Z3, Canada

<sup>b</sup> Laboratory for Alternative Energy Conversion (LAEC), School of Mechatronic Systems Engineering, Simon Fraser University, Surrey, BC V3T 0A3, Canada

<sup>c</sup> Institute for Integrated Energy Systems and Energy Systems and Transport Phenomena Lab (ESTP), Department of Mechanical Engineering, University of Victoria, Victoria, BC V8W 3P6, Canada

<sup>d</sup> Vancouver International CleanTech Research Institute, 4475 Wayburne Dr. Suite 310, Burnaby, BC V5G 4X4, Canada

## ARTICLE INFO

### Article history:

Received 23 July 2015

Received in revised form

8 March 2016

Accepted 9 March 2016

Available online 30 March 2016

### Keywords:

Contact resistance

Porosity

Micro porous layer (MPL)

Gas diffusion layer (GDL)

Fuel cells

## ABSTRACT

The present study reveals that the conventional notion that thermal contact resistance increases with porosity does not necessary hold. It is proved through a mechanistic robust model that, under specific circumstances, the porosities of two contacting bodies attain a critical value beyond which the contact resistance counter-intuitively drops. The model focuses on micro porous layers (MPLs) coated on gas diffusion layers (GDLs) of polymer electrolyte membrane fuel cells (PEMFCs) and is validated with the MPL-GDL thermal contact resistance measured over a range of pressure.

The counter-intuitive reduction of the contact resistance with porosity can find important applications in energy conversion systems such as PEMFCs and batteries where contact resistance plays a major role in ohmic loss and heat management. This game-changing finding can lead to improving mass and heat transfer, diffusivity and permeability of porous materials by increasing the porosity without any compromise on contact resistance or ohmic loss. The present cutting-edge research can also open new avenues for fuel cell and any other manufacturers to develop state-of-the-art materials with higher porosities but lower contact resistances, which are currently not available in the market.

Copyright © 2016, Hydrogen Energy Publications, LLC. Published by Elsevier Ltd. All rights reserved.

\* Corresponding author. Department of Chemical and Biological Engineering, University of British Columbia, 2360 East Mall, Vancouver, BC V6T 1Z3, Canada. Tel.: +1 (778) 782 8587; fax: +1 (778) 782 7514.

E-mail addresses: [hsf@mail.ubc.ca](mailto:hsf@mail.ubc.ca), [hsf@chbe.ubc.ca](mailto:hsf@chbe.ubc.ca), [hamidreza.sadeghifar@ubc.ca](mailto:hamidreza.sadeghifar@ubc.ca), [sadeghif@sfu.ca](mailto:sadeghif@sfu.ca), [h\\_sadeghifar@alum.sharif.edu](mailto:h_sadeghifar@alum.sharif.edu) (H. Sadeghifar).

<http://dx.doi.org/10.1016/j.ijhydene.2016.03.073>

0360-3199/Copyright © 2016, Hydrogen Energy Publications, LLC. Published by Elsevier Ltd. All rights reserved.

## Introduction

Contact or interfacial resistance plays a major role in ohmic loss and electrical and heat management of energy conversion systems such as fuel cells, batteries and capacitors comprised of microstructural porous materials [1–3]. This interfacial resistance, together with the bulk transport properties, is a strong function of porosity [4–6]. A high porous material provides higher heat [7] and mass transfer, diffusivity and permeability but also higher contact resistance and ohmic loss [8,9]. This crucial trade-off dramatically influences heat, electron and ion transfer in fuel cells and batteries. Contact resistance (ohmic loss) reduction and heat transfer, diffusivity and permeability improvement are simultaneously favored in energy conversion devices [10]. However, no reduction of contact resistance with porosity has been to date reported. All attempts have failed to resolve the tradeoff between porosity-based transport properties and contact resistance (or ohmic loss).

The aim of this study is to explore the possibility of contact resistance (or ohmic loss) reduction with porosity through a mechanistic robust model. The focus will be on the interface of two widely-used carbon-based porous materials: a fibrous porous medium called gas diffusion layer substrate and its neighboring micro porous layer (MPL) (see Fig. 1) of polymer electrolyte membrane fuel cells (PEMFCs). The MPL carbon

particles clusters and their contact with one fiber are schematically illustrated in Fig. 2. The present model allows the systematic investigation of the effect of GDL and MPL porosities on their contact resistance and provides insights and guidance for the development of new and improved materials for energy conversion systems.

## Model development

### Geometrical model

A schematic of the contact between spherical carbon particles of an MPL and cylindrical carbon fibers of a GDL is shown in Fig. 3. The random distance between the fibers of the GDL surface [11] and the carbon particles of the MPL surface are exaggeratedly illustrated in Fig. 3. This figure also shows some ellipses as the contact areas between one fiber and several carbon particles. The assumptions of the proposed model include: 1) steady state heat transfer; 2) constant thermo-physical properties; 3) cylindrical GDL fibers; 4) spherical MPL carbon particles; 5) elastic deformation; 6) static mechanical contact, i.e., no vibration effects; and 7) short-range surface forces are negligible (Hertz/Surface forces  $\approx 10^2$  for carbon particle-fiber contacts) [12–14]. The geometrical equations and parameters of the GDLs and MPLs required in the present model are summarized in Table 1. Further details on the

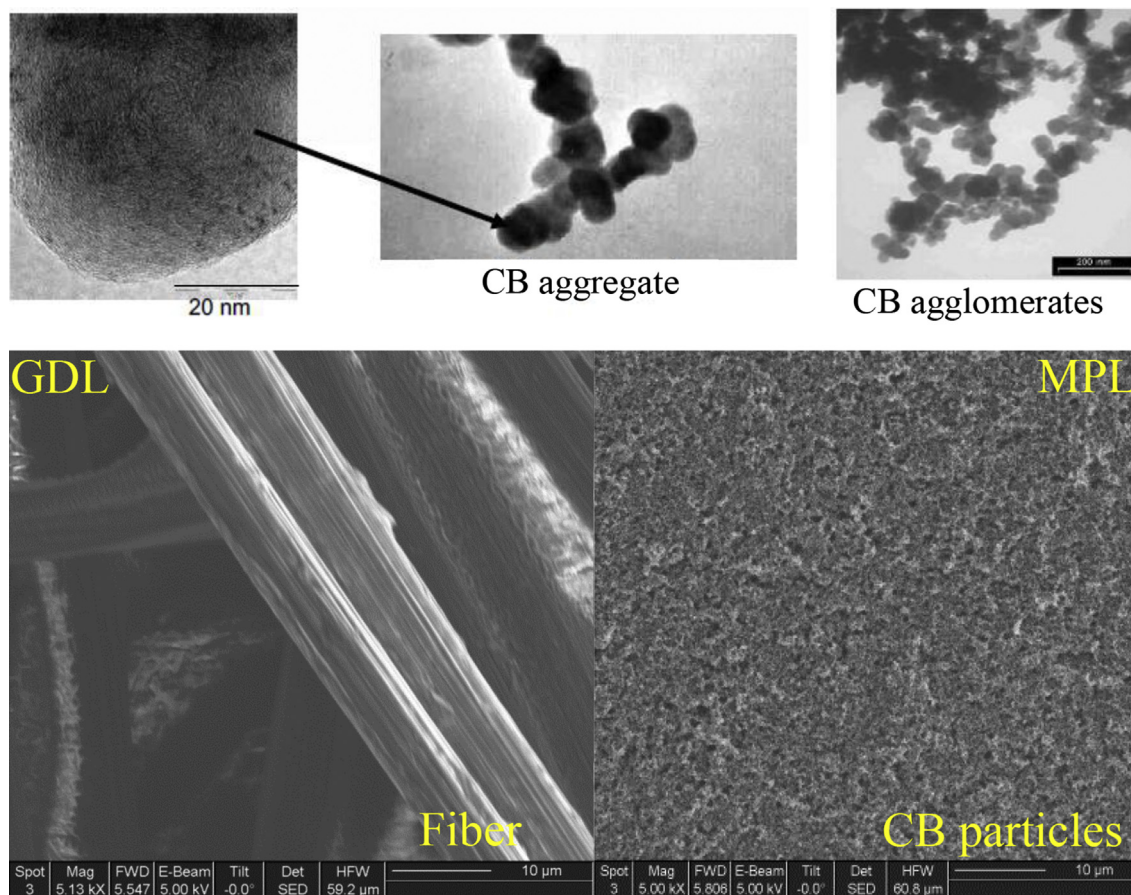


Fig. 1 – Images of an SGL MPL-GDL 24BC surfaces (present study) and MPL carbon black (CB) agglomerates, clusters and particles [25].

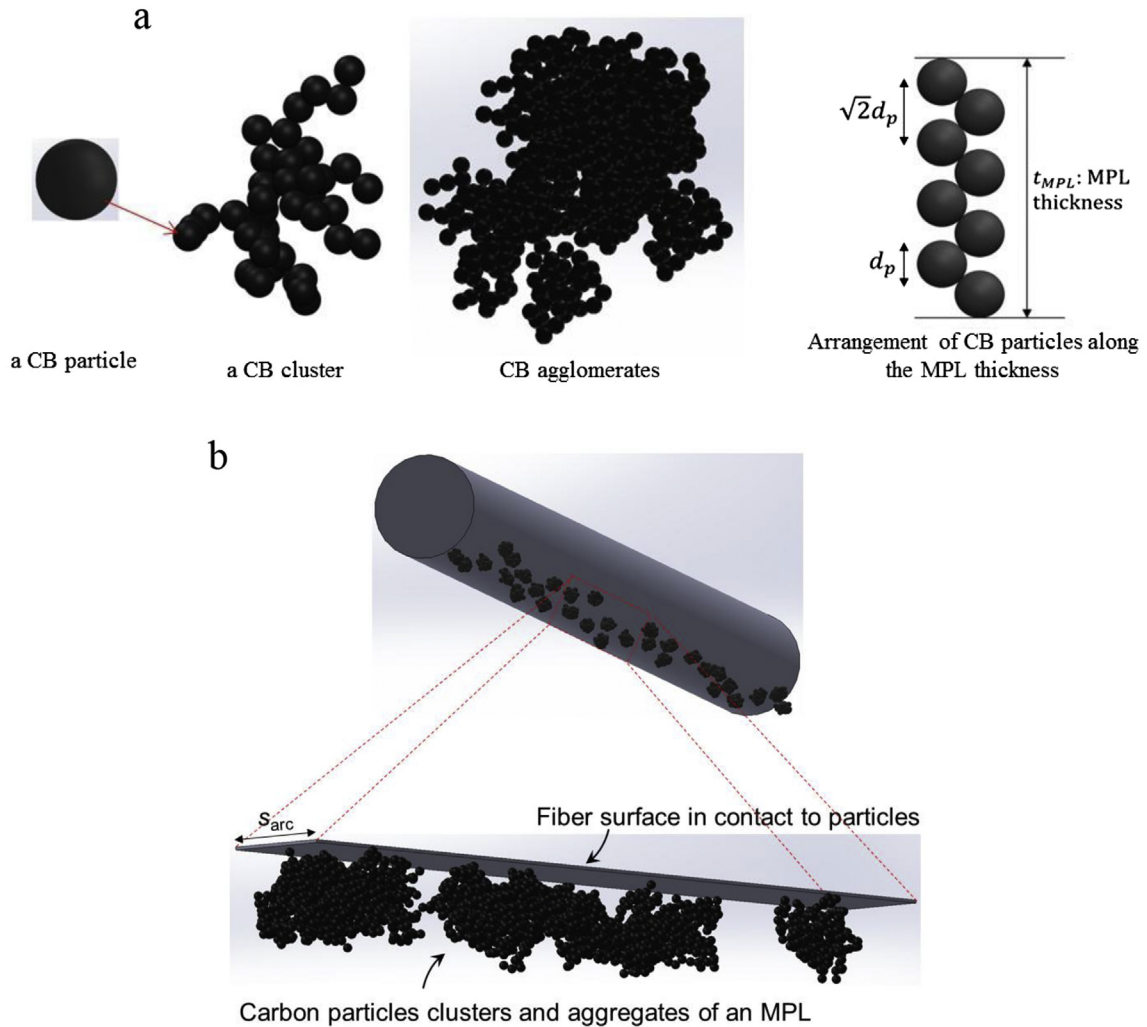


Fig. 2 – (a): Geometrical modeling of spherical carbon particles arrangement inside an MPL: The number of MPL carbon particle layers can be obtained as  $\frac{\sqrt{2}t_{MPL}}{d_p}$ . (b): MPL carbon particles clusters and agglomerates, as the unit components of an MPL, contacting fibers (not to scale for the purpose of illustration); only carbon particles on the MPL surface touch the GDL fibers.

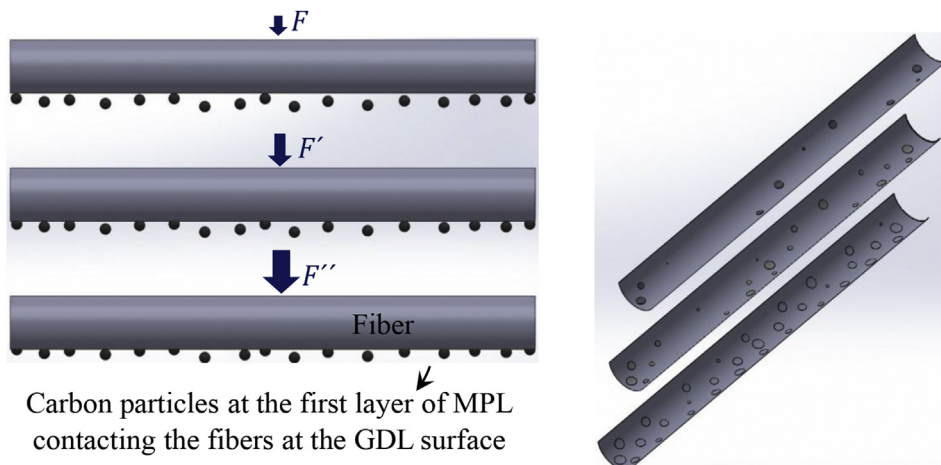


Fig. 3 – MPL carbon particles in contact with a GDL fiber: Increasing pressure ( $F < F' < F''$ ) increases the number and contact area of Hertzian contact ellipses (the size of particles and contact areas have been exaggerated for clarity).

structure and composition of the GDL and MPL surfaces can be found in “Supplementary Materials A”.

### Mechanical model

Heat transfers from one GDL fiber to MPL carbon particles through the contact spots at the interface and the resistance to heat conduction depends on the contact area dimensions, which are summarized at the end of Table 2. GDL surfaces have a random distribution of surface asperities (see Ref. [15]). Following Mikic [16] and Bahrami et al. [15,17], a Gaussian distribution of spacings between fibers and the MPL surface is assumed, which is a function of pressure:

$$n_s = \frac{1}{16} \left( \frac{m}{\sigma} \right)^2 \frac{\exp(-2\gamma^2)}{\operatorname{erfc}(\gamma)} A \quad (16a)$$

$$\gamma = \operatorname{erfc}^{-1} \left( \frac{4P}{H_{el}} \right) \quad (16b)$$

where  $m$ ,  $\sigma$ ,  $\gamma$ ,  $A$ ,  $H_{el}$  and  $P$  are respectively asperity slope, surface roughness, apparent (total) area, elastic micro-hardness, and pressure (see Table 1). The number of fibers contacting the surface ( $N_f$ ) at a given pressure of  $P$  can be obtained by the same proportionality as Eq. (16) proposes:

**Table 2 – Hertzian equations of a sphere-cylinder and sphere-plane contact [12].**

Contact	Contact radius	Equation
Sphere-cylinder contact	$1 + \frac{d_p}{d_f} = \frac{(1/k^2)E(k') - K(k')}{K(k') - E(k')}$	(14a)
	$k' = \sqrt{1 - k^2}$	(14b)
	$b = \sqrt[3]{\frac{3FkE(k')}{4\pi E^*} \left( \frac{1}{d_p} + \frac{1}{d_f} \right)^{-1}} = ka$	(14c)
Sphere-plane contact	$a = b = \sqrt[3]{\frac{3Fd_p}{8E^*}}$	(15)

$$\frac{N_f}{N_{ft}} = \frac{n_{sGDL}}{n_{stGDL}} \quad (17)$$

where  $N_{ft}$  is the total number of fibers as given in Table 1.  $n_{sGDL}$  is obtained at the pressure applied on the sample (e.g.,  $P = 2$ –20 bar) and  $n_{stGDL}$  at a pressure where the main gaps

**Table 1 – Geometrical specification and mechanical properties of fibers for typical GDLs.**

Symbol	Parameter	Units	Value or equation	Basis	Eq./Figure
$E$	Young modulus of fiber & MPL carbon particles	GPa	210 & 210 [2] [9]	Meas.	–
$\nu$	Poisson ratio of fiber & MPL carbon particles	–	0.3 & 0.3 [2] [9]	Meas.	–
$k$	Thermal conductivity of fiber & MPL carbon particles	W m <sup>-1</sup> K <sup>-1</sup>	115 [21] & 1.5 [16]	Meas.	–
$l_{fap}$	GDL apparent fiber length	μm	3000 [6]	Meas.	–
$d_f$	GDL fiber diameter	μm	7.5 [6], 8.5 [9]	Meas.	–
$d_p$	MPL carbon particle diameter	nm	10–100	Meas.	Fig. 5
$\Delta$	Fiber amplitude	μm	4 $d_f$ [6]	Meas.	–
$\lambda$	Fiber wavelength	μm	50–1900 [6]	Meas.	–
$N_s$	Number of troughs of each fiber	–	$N_s = \frac{L_{fap}}{\lambda} + 1$	Derv.	(1)
$l_f$	GDL fiber length	m	$2(N_s - 1)\sqrt{\Delta^2 + \frac{\lambda^2}{4}}$	Derv.	(2)
$s_{arc}$	Arc length of fiber circumference that can come to contact to particles	m	$d_f \tan^{-1} \left( 2 \frac{d_p}{d_f} \sqrt{1 + \frac{d_p^2}{d_f^2}} \right)$	Derv.	(3)
$t_{MPL}$	MPL thickness	μm	45 [26]	Meas.	–
$\epsilon_{MPL}$	MPL porosity	–	0.42 (MPL mass = 0.029 gr)	Meas.	–
$\epsilon_{GDL}$	Nominal substrate porosities of GDLs SGL 24BA and 25BA	–	0.88 and 0.92 [26]	Meas.	–
$N_{ft}$	Total number of fibers at the GDL surface	–	$\frac{4A(1-\epsilon_{GDL})}{\pi d_f l_f}$	Derv.	(4)
$N_{pt}$	Total number of carbon particles at the MPL surface	–	$\frac{\sqrt{2}d_p A(1-\epsilon_{MPL})}{\frac{8}{3}\pi \left( \frac{d_p}{2} \right)^3}$	Derv.	(5)
$A$	GDL and MPL cross-sectional area (apparent surface area)	m <sup>2</sup>	0.000507	Meas.	–
$\psi_{acGDL}$	Active area percentage of a GDL surface at compression of $P$	m <sup>2</sup> /m <sup>2</sup>	$\frac{(N_f l_f s_{arc})(1-p_{GDL}^{TFF})}{A}$	Derv.	(6)
$\psi_{acMPL}$	Active area percentage of an MPL surface at compression of $P$	m <sup>2</sup> /m <sup>2</sup>	$\frac{(N_p \frac{\pi d_p^2}{4})(1-p_{MPL}^{TFF})}{A}$	Derv.	(7)
$p_{\psi\psi}$	GDL-MPL solid-phase contact probability	–	$\psi_{acMP} L \times \psi_{acGDL}$	Calc.	(8)
$N_p - 1f$	Total number of carbon particles that come into contact to one fiber	–	$\frac{p_{\psi\psi} N_p}{N_f}$	Derv.	(9)
$\sigma_{GDL}$	Roughness of GDLs SGL 24BA & SGL 25BA	μm	17, 31 [27]	Meas.	–
$m_{GDL}$	Asperities slope for GDL	–	0.076 $\sigma_{GDL}^{0.52}$ [15] [22]	Calc.	(10)
$H_{el GDL}$	Effective elastic modulus	Pa	$\frac{E^* m_{GDL}}{\sqrt{2}}$ [15] [22]	Calc.	(11)
$\sigma_{MPL}$	MPL roughness of GDLs SGL 24BA & SGL 25BA	μm	2.5, 1.3 [27]	Meas.	–
$m_{MPL}$	Asperities slope for MPL	–	0.076 $\sigma_{MPL}^{0.52}$ [15] [22]	Calc.	(12)
$H_{el MPL}$	Effective elastic modulus	Pa	$\frac{E^* m_{MPL}}{\sqrt{2}}$ [15] [22]	Calc.	(13)



between consecutive fibers [18] disappear as a result of pressure. This pressure ( $P_{st}$ ) corresponds to the compression at which no practical change can be observed in the population density of the contact spots on a pressure indicating film [19] pressed against the sample, see “Supplementary Materials B”.

The number of MPL carbon particles that can contact all the fibers at a pressure of  $P$  is

$$\frac{N_p}{N_{pt}} = \frac{n_{sMPL}}{n_{stMPL}} \quad (18)$$

The number of MPL carbon particles contacting one GDL fiber will therefore be:

$$N_p^{sf} = \frac{N_p}{N_f} \quad (19)$$

### Thermal model

Due to the very small area of the contact ( $10^{-17}$ – $10^{-15}$  m<sup>2</sup>), the heat transferred from one GDL fiber to the MPL carbon particles encounters a large resistance, known as spreading/constriction resistance. According to Bahrami et al. [15,20], the total thermal contact resistance of non-conforming surfaces, here for one fiber, is a summation of the macrocontact and all the microcontact resistances:

$$R_{tot}^{f-MPL} = R_{mac}^{f-MPL} + R_{mic}^{f-MPL} \quad (20)$$

The spreading/constriction macrocontact resistance that occurs on each cylindrical fiber surface contacting the carbon particles of MPL can be obtained by Ref. [6]:

$$R_{mac}^{f-MPL} = \frac{1}{\pi l_f k_f} \ln \left( \frac{4d_f}{S_{arc}} \right) - \frac{1}{2l_f k_f} \quad (21)$$

where  $k_f$  is the thermal conductivity of fibers (=115 W/m K [2,6,21]). The microcontact resistance for each fiber is an inverse of the parallel summation of all the microcontact resistances created on its surface:

$$R_{mic}^{f-MPL} = \left( \sum_{i=1}^{N_p^{f-MPL}} \frac{1}{R_{mic_i}^{f-p}} \right)^{-1} \quad (22)$$

where  $R_{mic_i}^{f-p}$  is the spreading/constriction resistance between one fiber and one arbitrary carbon particle contacting that fiber:

$$R_{mic_i}^{f-p} = R_{mic_i}^f + R_{mic_i}^p \quad (23)$$

Since  $a$  and  $b$  are much smaller than the fiber diameter ( $a/d_f \sim 10^{-3}$ ), the concept of heat transfer on a half space is used for the fiber side of any fiber-particle contact [2,6]:

$$R_{mic_i}^f = \frac{1}{2\pi k_f a} \int_0^{\frac{\pi}{2}} \frac{dt}{\sqrt{1 - \eta^2 \sin^2 t}} \quad (24)$$

$$\eta = \frac{1}{\sqrt{1 - \left(\frac{b}{a}\right)^2}} \quad (25)$$

And for the particle side, since  $a \approx b$  (circular contact spots) and the fibers can be considered as flat surface against the small particles of MPL, the equation of smooth sphere-flat contact can be employed [15,22,23]:

$$R_{mic_i}^p = \frac{\left(1 - \frac{2a}{d_p}\right)^{1.5}}{2 \left(\frac{2k_f k_p}{k_f + k_p}\right) a} \quad (26)$$

where  $k_p$  is the thermal conductivity of carbon particles (=1.5 W/m K [16,24]). The thermal contact resistance between the GDL and MPL for one carbon particle diameter can be obtained as:

$$TCR_{d_{pj}} = \frac{R_{tot}^{f-MPL}}{N_f} \quad (27)$$

Ultimately, the TCR between the GDL and MPL is the TCRs of different carbon particle diameters (Eq. (27)) averaged based on their occurrence probability in an MPL:

$$TCR = \sum_{j=1}^{n_{ptotal}} p_{d_{pj}} TCR_{d_{pj}} \quad (28)$$

where  $p_{d_{pj}}$  is the probability of occurrence of each particle diameter ( $d_{pj}$ ) already provided in “Supplementary Materials A”.

## Results and discussion

### Model validation

The interfacial thermal resistances of the MPL-coated type of the GDL substrates SGL 24BA and 25BA were measured in the previous work of the same authors [5]. Fig. 4 compares the present model with the experimental GDL-MPL contact resistances for these GDLs. The model results are in acceptable agreement with the experimental data and the model well captures the trend of the experimental TCRs over a wide range of pressure. Fig. 4 also shows that, as mentioned earlier, the model result is not sensitive to  $P_{st}$ .

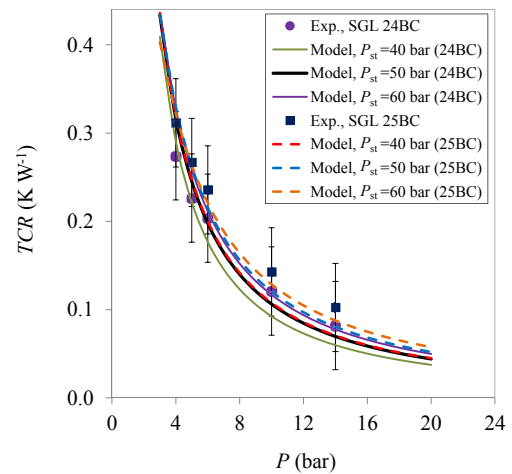


**Fig. 4 – Comparison of the present model with experimental data for SGL 24BC and 25BC:  $P_{st}$ , the compression at which all fibers can come into contact to the MPL surface, is a constant parameter to which the model is not sensitive, but the model is sensitive to varying compression  $P$  (fuel cell stack clamp pressure).**

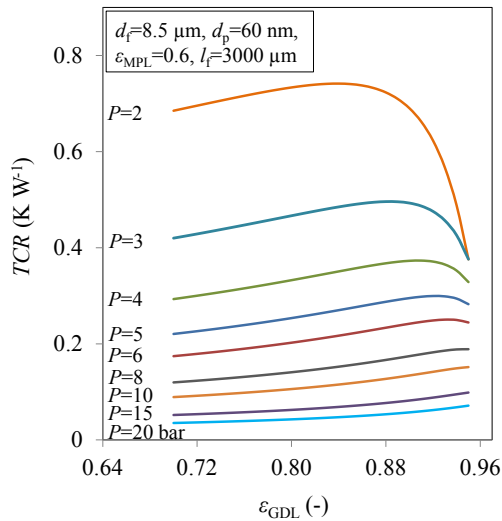


**Fig. 5 – Effect of GDL porosity on the TCR at three different pressures: a critical porosity ( $\epsilon_{GDL\ cr}$ ) of approximately 86% is observed at the low pressure of 2 bar. With increasing the pressure, the critical porosity increases and at high pressures, it may disappear.**

#### Effect of GDL porosity ( $\epsilon_{GDL}$ ) on TCR

The influence of GDL porosity on the TCR plotted in Fig. 5 reveals that TCR is more sensitive to porosity at lower pressures and higher range of porosities. It is visible from Fig. 5 that increasing the pressure reduces its impact on the TCR, irrespective of the GDL porosity. One important point to notice here is that TCR counter-intuitively decreases beyond a porosity of approximately 86% at the low pressure of 2 bar. Overall, at low pressures, there can be a critical porosity beyond which the TCR may decrease. This can be attributed to the tradeoff between the size of each contact spot (Fig. 6a) and the number of contact spots (Fig. 6b).

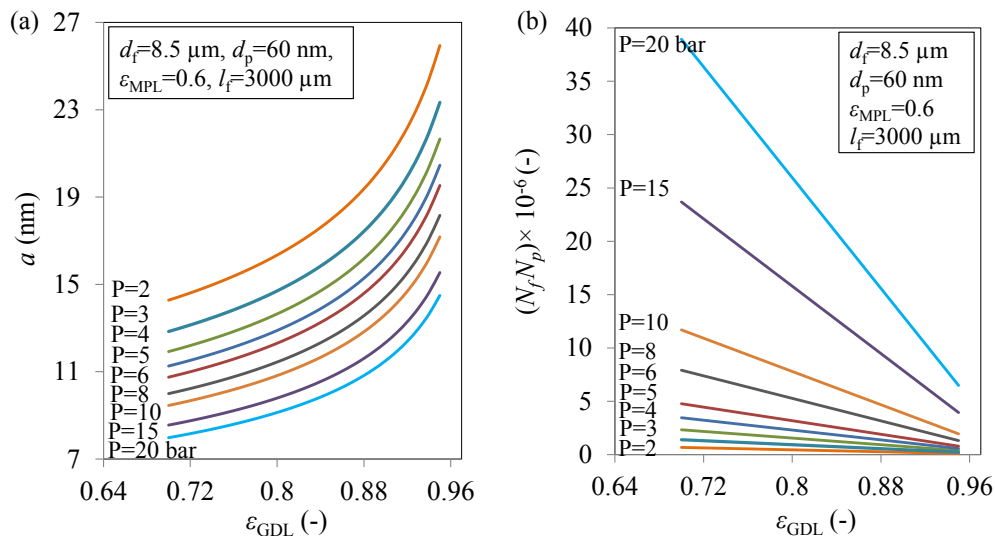


**Fig. 6 – Variations of the radius of each contact spot (a) and the number of contact spots (b) with the GDL porosity.**

It is well known that the size and the number of contact spots determine the TCR. For a fixed pressure, the radius or size of contact spots decreases with their population (Fig. 6a) since the force divided between more spots will be lower. This effect is more pronounced at lower number of contact spots, i.e., higher porosities and lower pressure as shown in Fig. 6a. (e.g., compare a change from 1 to 2 spots with a change from 1 million to one million and one (or even one million and a few thousands) spots). In other words, for typical GDLs porosities, the number of fibers is so high that any reduction in it (as a result of the porosity increase) can lead to little increase in the size of the contact spots and, hence, TCR increases with porosity. However, as the GDL porosity approaches very high values close to unity, the number of contact spots (Fig. 6b) becomes so low that the effect of the spots size growth on the TCR becomes competitive with, and beyond specific (critical) values of porosity (see Fig. 5), dominant over, the effect of the spots population. This effect becomes more critical at lower pressures where the number of contact spots is (much) lower (Fig. 6b). For this reason, as shown in Fig. 5, with increasing pressure, higher critical porosities are observed and at very high pressure, the critical porosity (peaks) may disappear. This is an important trend that may be used for GDL manufacturing and fuel cell design. Finding this novel concept of the contact resistance reduction with porosity can help fuel cell and any other manufacturers develop new state-of-the-art materials with higher porosities but lower contact resistances. At the present, such materials are not available in the market.

#### Effect of MPL porosity ( $\epsilon_{MPL}$ ) on TCR

Fig. 7 shows that the trends of the TCR variations with MPL porosity are similar to the ones observed for the case of GDL porosity, i.e., Fig. 5. At lower pressures, the effect of porosity on the TCR is more pronounced and with increasing pressure, the effect decreases and an almost linear trend is observed at the high pressure of 20 bar. At the pressure of 2 bar, a reduction in TCR is observed with increasing MPL porosity to values

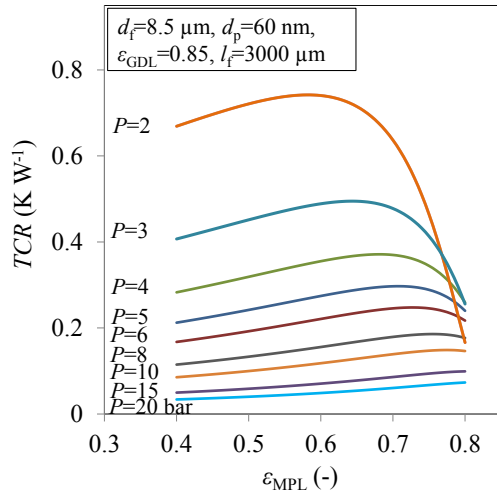


**Fig. 7 – Effect of MPL porosity on the TCR at three different pressures: a critical porosity ( $\epsilon_{MPL\ cr}$ ) of approximately 60% is observed at the low pressure of 2 bar. With increasing the pressure, the critical porosity increases and at high pressures, it may disappear.**

higher than 0.60. A similar trend was observed in Fig. 5 for the same pressure. In other words, as MPL porosity goes up, the contact spot radius  $a$  increases and the number of contact points decreases, which lead to the appearance of a maximum value for the TCR for a wide range of pressure (Fig. 7). This is because with increasing MPL porosity beyond certain values ( $>0.6$ ), the rate of the growth of each contact area, or the rate of decreasing of the TCR at each contact spot, becomes higher than the rate of reduction in the number of contacts. This important finding can be implemented for the design and manufacturing of fuel cells, GDLs, MPLs, and in general, any other porous materials.

## Summary and conclusion

Through robust mechanistic modeling, it was shown that the conventional notion that contact resistance increases with porosity does not necessary hold. Under certain circumstances, a critical porosity value is reached when the trend is reversed making it possible for the contact resistance between two mating porous materials to drop with porosity. The critical values of the dominant parameters, determined by the model, provide reference values for GDL manufacturing and design for improving the heat/electrical management of polymer electrolyte membrane fuel cells. The novel finding of contact resistance reduction with porosity brings the potential for improving mass and heat transfer, diffusivity and permeability of porous materials by increasing the porosity without any increase in contact resistance or ohmic loss.

## Acknowledgments

The authors gratefully acknowledge the financial support of the Natural Sciences and Engineering Research Council of

Canada (NSERC). The first author also thanks Alireza Akhgar from the Department of Mechanical Engineering at the University of Victoria for technical guidance on the image analyses using the “ImageJ” software. The SEM and EDX images were taken using 4D LABS facilities at SFU.

## Nomenclature

$a$	Major radius of contact area between one fiber and one carbon particle, m
$b$	Minor radius of contact area between one fiber and one carbon particle, m
Calc.	Based on calculations
Derv.	Derived parameter or equation
$u$	Half of the width of the rectangular channel area, m
$F$	Force exerted on the entire GDL, N
Exp.	experimental value
$E$	Young's modulus, Pa
$F$	Force, N
$d_f$	GDL fiber diameter, m
$d_p$	MPL carbon particle diameter, m
$A$	GDL cross-sectional area, $m^2$
$A_{fp}$	The area of that part of each fiber surface that MPL carbon particles come in contact with, $m^2$
$l_{fap}$	Apparent fiber length, m
$N_s$	Number of troughs each fiber has
$N_f$	Number of fibers contacting the MPL surface at a pressure of, $P$
$N_p$	Number of carbon particles that can contact all the fibers at a compression of, $P$
$N_p^{1f}$	Number of carbon particles that can contact all the fibers at a compression of, $P$ per one fiber
$N_p - 1f$	Number of carbon particles that may contact one fiber at a compression of, $P$
$E^* = \left( \frac{1-\nu_c^2}{E_c} + \frac{1-\nu_f^2}{E_f} \right)$	Effective elastic modulus, Pa
$N_{ft}$	Total number of fibers
GDL	Gas Diffusion Layer
$l_{f\ real}$	Real fiber length, m
$k$	Thermal conductivity, $Wm^{-1}K^{-1}$
Meas.	Measured value or parameter
$n_s$	Number of asperities contacting the surface of another body in contact
$n_{st}$	Total number of asperities
PEMFC	Polymer electrolyte membrane fuel cell
$P$	Pressure on the entire GDL, Pa
$P_{st}$	Pressure at which all the fibers contact the surface
$p$	probability
$p_{d_{pj}}$	Probability of having carbon particles with a diameter of $d_{pj}$
$R$	Thermal resistance, $KW^{-1}$
$R_c$	Spreading/constriction resistance on cylinder side resistance, $KW^{-1}$
$R_f$	Spreading/constriction resistance on flat surface side, $KW^{-1}$
TCR	Thermal resistance correction, $KW^{-1}$
$TCR_A$	Thermal contact resistance per unit area, $KW^{-1}m^{-2}$
$t$	thickness, m

Greek letter

$\Delta$	Amplitude of fiber waviness, m
$\lambda$	Wavelength of fiber waviness, m
$\gamma$	Non-dimensional separation
$\epsilon$	Porosity
$\sigma$	GDL roughness, m
$\psi$	Active area percentage of GDL (MPL) surface that can come to contact to MPL (GDL)
$\nu$	Poisson's ratio

#### Superscript

$f - \text{MPL}$	Contact between one fiber and MPL carbon particles
$f - p$	Contact between one fiber and one carbon particle

#### Subscript

C	Cylinder
cr	Critical value
el	Elastic
f	Fiber
F	Flat surface
GDL	GDL or related to GDL
i	Carbon particle i
j	Carbon particle with the diameter of $d_{pj}$
m	Measured
mac	Macro
max	Maximum value
mic	Micro
min	Minimum value
MPL	MPL or related to MPL
n	Summation index
p	Carbon particles of MPL
t	Total value
tot	Total resistance
??	Related to probability of active areas of GDL and/or MPL that may come to contact

## Appendix A. Supplementary data

Supplementary data related to this article can be found at <http://dx.doi.org/10.1016/j.ijhydene.2016.03.073>.

## REFERENCES

- [1] Cozzolino R, Cicconardi SP, Galloni E, Minutillo M, Perna A. Theoretical and experimental investigations on thermal management of a PEMFC stack. *Int J Hydrogen Energy* 2011;36(13):8030–7.
- [2] Sadeghifar H, Bahrami M, Djilali N. A statistically-based thermal conductivity model for fuel cell gas diffusion layers. *J Power Sources* Jul. 2013;233:369–79.
- [3] Torkavannejad A, Sadeghifar H, Pourmahmoud N, Ramin F. Novel architectures of polymer electrolyte membrane fuel cells: efficiency enhancement and cost reduction. *Int J Hydrogen Energy* 2015;40(36):12466–77.
- [4] Singdeo D, Dey T, Ghosh PC. Contact resistance between bipolar plate and gas diffusion layer in high temperature polymer electrolyte fuel cells. *Int J Hydrogen Energy* 2014;39:987–95.
- [5] Sadeghifar H, Djilali N, Bahrami M. Effect of polytetrafluoroethylene (PTFE) and micro porous layer (MPL) on thermal conductivity of fuel cell gas diffusion layers: modeling and experiments. *J Power Sources* 2014;248:632–41.
- [6] Sadeghifar H, Djilali N, Bahrami M. A new model for thermal contact resistance between fuel cell gas diffusion layers and bipolar plates. *J Power Sources* 2014;266:51–9.
- [7] Sadeghifar H, Djilali N, Bahrami M. A compact closed-form Nusselt formula for laminar longitudinal flow between rectangular/square arrays of parallel cylinders with unequal row temperatures. *Int J Therm Sci* 2016;100:248–54.
- [8] Sadeghifar H, Djilali N, Bahrami M. Thermal conductivity of a graphite bipolar plate (BPP) and its thermal contact resistance with fuel cell gas diffusion layers: effect of compression, PTFE, micro porous layer (MPL), BPP out-of-flatness and cyclic load. *J Power Sources* 2015;273:96–104.
- [9] Sadeghi E, Djilali N, Bahrami M. Effective thermal conductivity and thermal contact resistance of gas diffusion layers in proton exchange membrane fuel cells. Part 1: effect of compressive load. *J Power Sources* Jan. 2011;196(1):246–54.
- [10] Chang WR, Hwang JJ, Weng FB, Chan SH. Effect of clamping pressure on the performance of a PEM fuel cell. *J Power Sources* 2007;166:149–54.
- [11] Sadeghifar H. Reconstruction and analysis of fuel cell gas diffusion layers using fiber spacing rather than pore size data: questioned validity of widely-used porosity-based thermal conductivity models. *J Power Sources* 2016;307:673–7.
- [12] Palaci I. Atomic force microscopy studies of nanotribology and nanomechanics. PhD Thesis. Switzerland: École Polytechnique Fédérale De Lausanne; 2007.
- [13] Brunner R, Tyndall GW, Waltman RJ, Talke FE. Adhesion between surfaces separated by molecularly thin perfluoropolyether films. *Tribology Lett* 2010;40:41–8.
- [14] Johnson K. Contact mechanics. 1st ed. Cambridge University Press; 1987.
- [15] Bahrami M. Modeling of thermal joint resistance for rough sphere-flat contact in a vacuum. PhD Thesis. Waterloo, Canada: University of Waterloo; 2004.
- [16] Remediakis IN, Fyta MG, Mathioudakis C, Kopidakis G, Kelires PC. Structure, elastic properties and strength of amorphous and nanocomposite carbon. *Diam Relat Mat*. 2007;16:1835–40.
- [17] Bahrami M, Yovanovich MM, Culham JR. Thermal joint resistances of nonconforming rough surfaces with gas-filled gaps. *J Thermophys Heat Transf* 2004;18(3):326–32.
- [18] Norouzfard V, Bahrami M. Deformation of PEM fuel cell gas diffusion layers under compressive loading: an analytical approach. *J Power Sources* 2014;264:92–9.
- [19] Sensor expert. 2014. <http://www.sensorexpert.com/aboutus.php>. Madison, USA.
- [20] Bahrami M, Yovanovich MM, Culham JR. Thermal joint resistance of conforming rough surfaces with gas-filled gaps. *AIAA J Thermophys Heat Transf* 2004;18:318–25.
- [21] Zamel N, Astrath NGC, Li X, Shen J, Zhou J, Astrath FBG, et al. Experimental measurements of effective diffusion coefficient of oxygen-nitrogen mixture in PEM fuel cell diffusion media. *Chem Eng Sci* 2010;65:931–7.
- [22] Yovanovich M, Marotta E. "Thermal spreading and contact resistance," in *heat transfer handbook*. In: Bejan A, Kraus AD, editors. New York: Wiley; 2003.
- [23] Bahrami M, Yovanovich MM, Culham JR. Effective thermal conductivity of rough spherical packed beds. *Int J Heat Mass Transf Sep*. 2006;49(19–20):3691–701.
- [24] Bullen AJ, O'Hara KE, Cahill DG, Monteiro O, von Keudell A. Thermal conductivity of amorphous carbon thin films. *J Appl Phys* 2000;88:6317–20.



- 
- [25] Bellinghen ChVan, Probst N, Grivei E, Ciallella C. Additives for electrical and thermal conductivity. In: BPRI meeting on additives. Gent; 2008.
- [26] SGL Group – the Carbon company. SIGRACET diffusion media, manufacture data sheet. Web: <http://www.sglgroup.com/cms/international/home>
- [27] El-Kharouf A, Mason TJ, Brett DJL, Pollet BG. Ex-situ characterisation of gas diffusion layers for proton exchange membrane fuel cells. *J Power Sources* 2012;218:393–404.